REGULAR PAPER

High-Speed Milling of Hardened Mold Steel P20 with Minimum Quantity Lubrication

Shixiong Wu[1] · Hongchang Liao[1] · Suyang Li[1] · Jundong Bi[1] · Zhiyang Li[1]

Abstract

Strong thermal–mechanical coupling and rapid tool failure easily occur in the milling process of hardened steel with solid end mills. This work investigates the effectiveness of minimum quantity lubrication (MQL) during high-speed milling of hardened mold steel. Three kinds of spraying modes were designed in the experiment. They are namely the spraying ways to the flank face (MQL-F), to the rake face (MQL-R) and to the rake and flank faces (MQL-FR). The cutting forces, tool wear, and chips when using the MQL modes and compressed air cooling mode (CAIR-F) were compared, and the wear mechanism and lubrication mechanism were further analyzed. The results showed that the tool wear values and milling forces of several MQL modes were significantly lower than those with CAIR-F. The milling force and tool wear values were successively reduced using MQL-R, MQL-F, and MQL-FR, with better lubrication of the rake face resulting in a smaller curvature radius for the chip. Abrasion wear, adhesion/attrition wear, and flaking/chipping were the main wear mechanisms. The MQL-FR method was the optimal method of the MQL modes. It could effectively reduce the cutting contact stress and unit cutting energy, and obviously reduced wear phenomena such as adhesion and chipping.

Keywords Hardened steel · High-speed milling · MQL · Solid end mill

1 Introduction

Hardened steel is a material with high hardness (50–70 HRC), good wear resistance, and good mechanical properties, which give it a wide range of applications in mold manufacturing. Milling is a typical processing method for hardened steel molds. In recent years, with the development of high-speed machining technology, high-speed milling has often been used in mold processing [1]. Because of the characteristics of hardened steel materials, the cutting edges in high-speed milling are subjected to a large impact force and high cutting temperature, which can easily cause the cutting edge to become worn and damaged, shortening the tool life [2]. Therefore, methods to control the cutting heat and force, and extend the tool life through cooling and lubrication, have become key scientific issues worth studying in relation to the high-speed milling of hardened steel.

Some enterprises use emulsified cutting fluids in their cutting operations. Although this type of cutting fluid has a good cooling effect and a certain lubricating effect, the use of such a cutting fluid causes several problems, including a negative impact on human health and the environment [3]. Using and recycling the cutting fluid also has a high cost, which can reach or exceed 7–14% of the total manufacturing cost [4]. Moreover, a low cutting fluid flow rate is used, which makes it difficult for it to enter the tool–chip or tool–workpiece contact interface. These effects make the use of this type of fluid unsatisfactory in the high-speed milling of hardened steel [5].

Environmentally friendly green cooling lubrication methods are an inevitable development direction for sustainable manufacturing due to environmental issues, cost issues and government regulations [6]. Some researchers have conducted green cutting research with four main types of methods. The first one is dry cutting; the second is cutting under compressed air cooling; the third is cutting in ultra-low temperature or low temperature gas environment; and the fourth is MQL cutting.

Dry cutting, with convenient and non-polluting processing characteristics, does not require any cooling and

✉ Shixiong Wu
  151688386@qq.com

1 Mechanical and Electrical Engineering Institute, Guangdong University of Technology, Panyu Higher Education Mega Center, Guangzhou 510006, Guangdong, China

lubrication device. Although the coating technology has been greatly developed [7], dry cutting has a problem of rapid tool wear for the cutting applications of high heat and force coupling, such as the high-speed milling of hardened steel molds.

Compressed air cooling is a commonly used method for the high speed milling of hardened steel molds. The compressed gas can take away part of the cutting heat and blow away the chips to prevent them from thermally residing. Compared to dry cutting, compressed air cooling method can improve tool life to a certain extent. However, the tool wear of compressed air cooling method is still relatively fast in the process of high-speed cutting because the thermal removal capacity of the compressed air is not high [8]. There is still a certain gap between the requirements of enterprises to reduce tool loss.

Cutting in ultra-low temperature or low-temperature gas environment is often used for the difficult-to-work materials. There are some common gas, like liquid nitrogen gas (− 195 °C), supercritical carbon dioxide low temperature gas (− 65 °C) and 0 ~ − 60 °C low temperature gas. For the cutting of some special difficult-to-machine materials, such as titanium alloy [9], high-temperature alloy [10, 11], it is very effective to spray ultra-low or low temperature gas, which can effectively reduce cutting temperature, adhesive wear and plastic deformation of the cutting edge. And it also significantly delays the tool wear process and improves the surface quality of workpiece. However, this cooling method requires purchase and maintenance of an external air-conditioning device and consumes a large amount of cold air during cutting, thereby significantly increasing the processing cost. Due to processing cost issues, this method is currently used less in the actual machining of hardened steel molds.

MQL is a near-dry machining method with environmental and economical benefits. Carrying a small amount of atomized oil droplets, the compressed gas are sprayed onto the tool/chip/workpiece interfaces to delay tool wear and improve the quality of the machined surface [12, 13]. To prevent oil mist pollution, the flow rate of oil used is generally less than 100 mL/h. For 6061 aluminum alloy turning, Sreejih [14] compared three MQL methods, dry cutting and flooded coolant, and found that the tool wear of MQL was lower than the other two ways. Tawakoli et al. [15] studied the effect of MQL parameters on grinding. The results show that MQL grinding had less milling force and better surface quality than fluid grinding under certain parameters. In the study of Rahim and Sasahara [16], high speed drilling of Ti-6Al-4V was investigated under various coolant–lubricant conditions. It is said that MQL and flood conditions exhibited comparable performance in tool life, and the distinct tool wear characteristics of MQL drilling included adhesion and abrasion wear. The above research shows that MQL exhibits good cooling and lubrication effects in machining

such as turning, grinding and drilling, and can be used to replace traditional flood method.

Milling is an interrupted cutting method. MQL's machining characteristics such as cooling/lubrication and tool wear in milling are also different from turning or grinding in some respects. Two kinds of cutters are commonly used in milling: indexable mills and solid end mills. Several researchers have conducted MQL milling researches on indexable mills. In the MQL milling of nickel alloy, Zhang et al. [17] found that the life of indexable mill was prolonged by 57% compared with dry cutting. Cai et al. [18] and Liu et al. [19] studied the MQL milling of titanium alloy Ti-6Al-4V with indexable mill and found that the length of chipping edge, cutting force and surface roughness decreased with the increase of lubricating oil, but the injection angle had little effect on the processing. In the face milling study of Inconel 182, Wang et al. [20] found that the nozzle position and tool coat affected the cooling/lubrication effect of MQL. Milling studies of indexable mills have shown that MQL can achieve certain results in terms of extending tool life and improving surface quality.

The cutting edges of solid end mills are significantly different from indexable mills. The solid end mill has more cutting edges and they are spiral. Because of this geometric structure, the cutting process of solid end mill is much lighter, more stable and more efficient than indexable mill, so it is very suitable for fast feed high speed milling [21]. There are few MQL research literatures on solid end mills [22]. Iyappan and Ghost [23] studied the performance of solid end milling of aluminium alloy under dry and SQL environments. The experiment results indicated that SQL can eliminate the formation of BUE, reduce cutting force and surface roughness. The research results from Ganguli et al. [24] and Zhang et al. [25] showed that the application of MQL in solid end mill milling can prolong the tool life and reduce the milling force to a certain extent. However, these studies are based on shallow cutting style, that is, the axial cutting depth is small. In die milling with solid end mill, the cutting efficiency and tool life can be improved more effectively by using large axial cutting depth mode [1, 2]. Compared with the use of small axial depth of cut, the jet-flow is easily blocked by the workpiece and cutter and more difficult cover the cutting edge completely in the MQL milling process with the use of large axial depth of cut. For the high-speed milling with large axial depth of cut mode, it is necessary to carry out systematic research and understand the adaptability of MQL and the mechanism of cooling and lubrication. Hardened die steel is a difficult-to-work material in the mold producing process. High-speed milling with large axial depth of cut significantly improves the cutting efficiency of hardened steel mold, but the thermal-force coupling is

sharp and the tool wear is fast during the cutting process. If the application of MQL can effectively reduce the tool wear and improve the processing efficiency, it will have practical significance in industrial production. This paper will carry out this work. The characteristics and mechanism of tool wear, cutting force, chip formation, cooling and lubrication in the high-speed milling hardened die steel using solid end mills under MQL condition will be systematically studied in the study. Considering several aspects such as injection mode and oil flow rate, four MQL methods were designed. Under two sets of cutting parameters, four MQL modes are compared with the compressed air cooling mode. In the experiment, key characterization quantities, such as milling force, tool wear, tool breakage and chip, were compared and tested, and cooling/lubrication mechanism and tool wear mechanism under MQL condition were further analyzed. The rest of this article is as follows. Section 2 introduces workpiece, tool material and experimental process. Section 3 gives the experimental results and Sect. 4 discusses the experimental results. Finally, the conclusion is given in Sect. 5.

2 Experimental Procedure

The experimental conditions for the high-speed milling are listed in Table 1.

The processing machine was a MILLTAP 700 machining center, with a maximum spindle speed of 24,000 rpm and maximum spindle power of 6 kW. The workpiece material used in the experiment was P20 steel, which mainly consists of C, Mn, Cr, Mo, Si, P, and S. P20 steel has good mechanical and cutting properties, making it suitable for medium- and large-scale die making. The hardness of P20 steel after quenching is within the range of 55–57 HRC. The tool used in the experiment was a coated-carbide solid end mill, which is the most commonly used tool in solid end mills at present. The main coating elements of the tool were Ti, Al, Si, and N. The main elements of the tool matrix were C, W, and Co. In the experiment, two sets of cutting parameters were designed based on the milled parameters of the hardened steel recommended by the factory. One set of parameters included a higher cutting speed and feed rate ($V_c = 175$ m/min, $F = 700$ mm/min, parameter 1), and the other set included a slightly lower cutting speed and feed

Table 1 Experimental conditions

Machine	MILLTAP 700	
Workpiece material	P20 Steel composition	
	C(0.28–0.40), Mn(0.60–1.00), Cr(1.40–2.00), Mo(0.30–0.55), Si(0.20–0.80), P(<0.03), S(<0.03), and Fe	
Workpiece size	25×90×300 mm	
Heat treatment	Quenching	
Hardness	55–57 HRC	
Cutting tools	Carbide four-flute spiral end mills (Zhuzhou Cemented Carbide Cutting Tools Co., Ltd)	
Coating of tool	Ti, Al, Si, N	
Tool matrix material	C (2.7%), W (85.73%), Co (8.86%)	
Diameter	Φ8 mm	
Radial rake angle	10°	
Axial rake angle	45°	
Clearance angle	2°	
Helical angle	45°	
Number of teeth	4	
Model	HMX-4E-D8.0	
Cutting conditions	Parameter 1	Parameter 2
Cutting speed (V_c)	175 m/min	125 m/min
Feed rate (F)	700 mm/min	625 mm/min
Radial depth of cut (A_e)	0.5 mm	0.4 mm
Axial depth of cut (A_p)	8 mm	8 mm
Environment	Compressed air cooling mode and four MQL modes	
Spraying angle approach	$\alpha_1 = 45°$, $\alpha_2 = 30°$ (see Fig. 1)	
Flow rate of oil	16 mL/h, 32 mL/h	
Flow rate of air	90 L/min	
Air pressure	0.5 Mpa	

rate ($V_c = 125$ m/min, $F = 625$ mm/min, parameter 2). The material removal rates were the same for both sets of cutting parameters.

Three MQL injection modes are designed, as shown in Fig. 1. The nozzles sprays atomization gas to the tool from above the machined workpiece surface. If the nozzle sprays gas to the tool from above the unmachined workpiece surface, the jet flow is difficult to reach the cutting contact area because it is blocked by the unmachined surface. Considering that the flow rate of injected lubricating oil may have a significant influence on the cutting process, two lubricating oil flow rates of 16 ml/h or 32 ml/h were used in
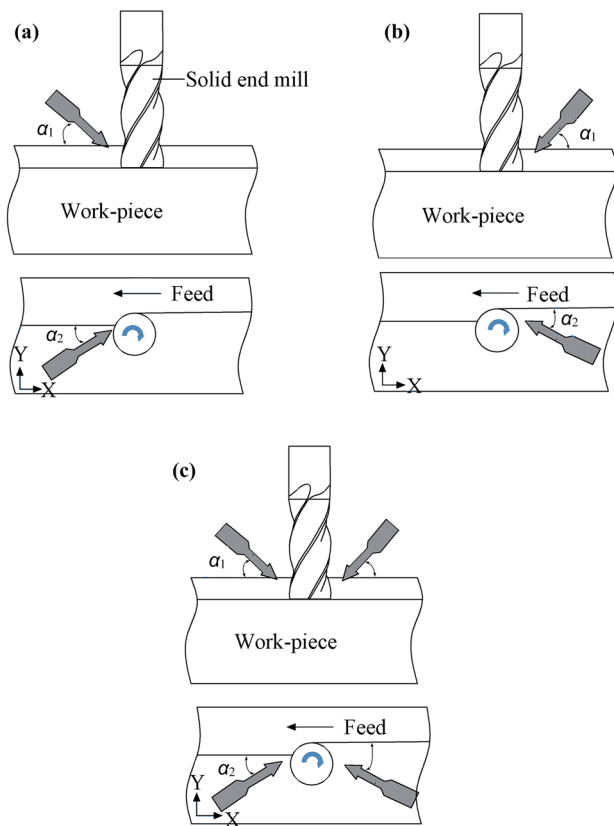
Fig. 1 MQL injection method. **a** Injection on the flank face (MQL-F), **b** Injection on the rake face (MQL-R), **c** Simultaneous injection on the flank face and rake face (MQL-FR)

the experiment. In the experiment, four MQL modes were finally designed (Table 2): MQL-F-16, MQL-R-16, MQL-F-32, and MQL-FR-16-16; here, "F" represents the flank face of the tool, and "R" represents rake face of the tool, while "16" and "32" represent the flow rates of the injected lubricating oil, i.e., 16 ml/h and 32 ml/h. The compressed air cooling method used a single nozzle to spray air to the tool flank face (CAIR-F). The MQL method and compressed air cooling method share the same equipment, thereby ensuring that the pressure and flow rate of the compressed gas used are consistent. When the lubricating oil passage is closed, the MQL method can be converted into a compressed air cooling method. The gas pressure and flow rate used for single-nozzle injection were 0.5 MPa and 90 L/min respectively. In order to reduce the power consumption of compressed gas, the compressed gas flow rate of each nozzle of the MQL-FR mode was reduced to 60 L/min.
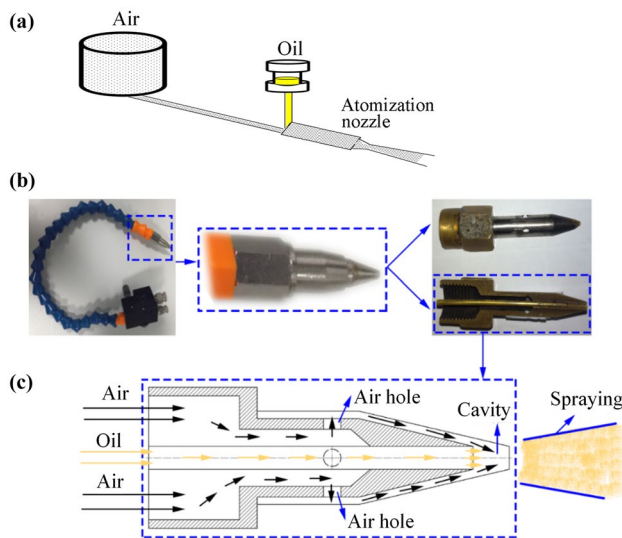
The principle of lubricating oil atomization of MQL is shown in Fig. 2. The lubricating oil is continuously conveyed to the nozzle along a pipe at a low flow rate, and the compressed gas is sent to the nozzle through another pipe. Then they both enter the nozzle annular cavity for atomization. Under the impact of high-rate compressed gas, the lubricating oil is dispersed into many micron fine oil mist particles and ejected from the nozzle to form MQL air jet. The lubricating oil used in MQL is a synthetic ester (2000-35), having a viscosity (40 °C) of 30 and a flash point of 300 °C.

In the high-speed milling process, the dynamic milling force was measured using a three-axis dynamometer (Kistler 9129AA) and a multi-channel charge amplifier (5080A). Tool wear was measured using a stereo microscope (Olympus-SZ61). The chip and cutting edge were quantified using a 3D scanner (Alicona Infinite Focus SL). The cutting edges of worn end mills were further analyzed by a scanning electron microscope (NanoSEM430) and an energy-dispersive spectroscopy (EDS).

Tool wear is usually characterized by the width of the flank wear land (VB). When the solid end mills reaches severe wear, there will often be cutting sparks, flat and broken chips, and the processing vibration is large. However, after the test, the average flank wear width was found to be less than the tool failure ISO criterion of VB = 0.3 mm.

Table 2 Five cooling modes designed in the milling experiment

Mode	Cooling and lubrication characteristics
MQL-F-16	The mist jet is sprayed toward the tool flank face by a single nozzle. The flow rate of the injected lubricating oil is16 ml/h
MQL-R-16	The mist jet is sprayed toward the tool rake face by a single nozzle. The flow rate of the injected lubricating oil is 16 ml/h
MQL-F-32	The mist jet is sprayed toward the tool flank face by a single nozzle. The flow rate of the injected lubricating oil is 32 ml/h
MQL-FR-16-16	Double nozzles respectively spray mist jets toward the rake face and flank face of the tool. The flow rate of the injected lubricating oil of each nozzle is 16 ml/h
CAIR-F	The compressive air is sprayed toward the tool flank face

Fig. 2 Atomization principle of MQL. **a** Atomization of compressed gas and lubricating oil transported through different pipelines, **b** Actual atomization nozzle, **c** Atomization process of lubricating oil in nozzle

Therefore, in this study, the milling force, chip shape, and machining spark in the later stage of machining are taken as the auxiliary reference, and the average flank wear value VB = 130 μm is set as the critical value of tool failure. When the average flank wear width of a tool reaches VB = 130 μm, the corresponding cutting time is the tool life value.

3 Experimental Results and Discussion

3.1 Tool Wear

Figure 3 shows the tool wear curves under the two sets of cutting parameters. Each curve consists of three stages: an initial rapid wear stage an intermediate stable wear stage, and a final rapid wear stage.

A comparison of Fig. 3a and b shows that the tool wear process was faster under the first set of parameters (parameter 1), which was related to the higher cutting speed and larger radial depth of cut used. Regardless of which set of parameters was used (parameter 1 or parameter 2), four MQL methods were used to effectively delay the change in the tool wear curve compared with the use of the compressed air cooling method. Four kinds of MQL methods, MQL-R-16, MQL-F-16, MQL-F-32, and MQL-FR-16-16, were used to successively reduce the degree of tool wear. When a single nozzle was used, the tool wear of the flank face injection mode (MQL-F-16) was lower than that of the tool face injection mode (MQL-R-16). The lubricating oil flow rates of MQL-F-32 and MQL-FR-16-16 were comparable, and they were both high oil flow rate modes.
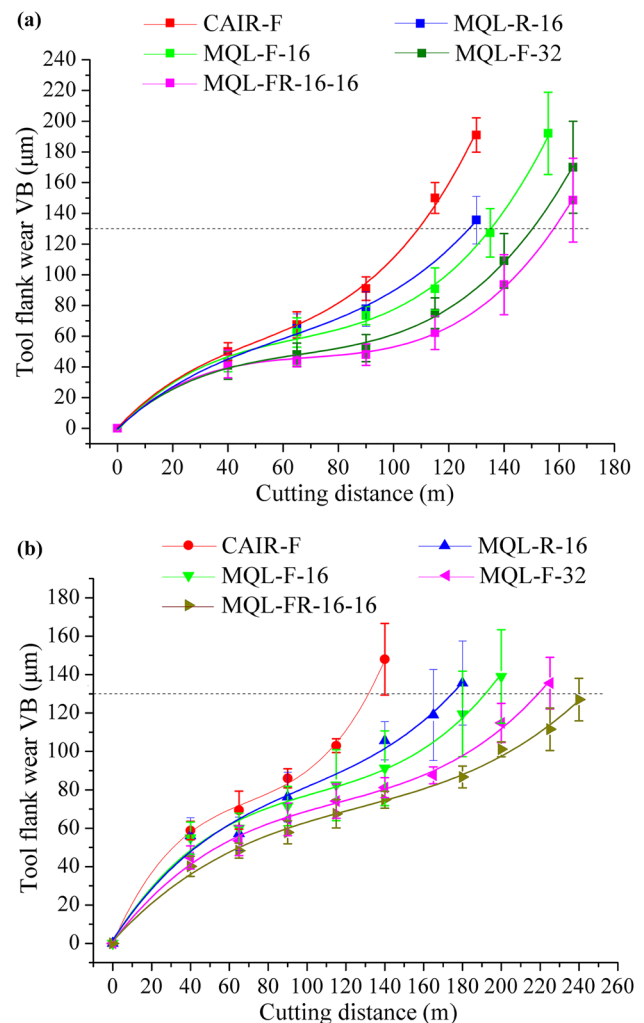
Fig. 3 Tool wear curves. **a** Comparison of tool wear curves under parameter 1, **b** Comparison of tool wear curves under parameter 2

Figure 3 shows that the tool wear values of the two high oil flow rate modes (MQL-F-32 and MQL-FR-16-16) are significantly lower than those of the two low oil flow rate modes (MQL-R-16 and MQL-F-16). In other words, increasing the flow rate for the lubricating oil had the significant effect of retarding the tool wear. In addition, the double-nozzle injection method (MQL-FR-16-16) had a slower tool wear than the single-nozzle (MQL-F-32) method, which indicated that the choice of injection mode under the same lubricating oil flow rate also had a significant impact on the tool wear process.

According to the aforementioned tool failure criteria, a horizontal line of vertical coordinate VB = 130 μm is constructed in Fig. 3. The horizontal line intersects the tool wear curve of each tool, and the abscissa of the intersection point is the final cutting distance of the tool. Further combined with the feed rate, the tool life value of each tool can be calculated.

Figure 4 shows the tool life comparison results for the two sets of cutting parameters. Under the conditions of cutting parameter 1, compared with the compressed air cooling mode CAIR-F, the four kinds of MQL modes, MQL-R-16, MQL-F-16, MQL-F-32, and MQL-FR-16-16, improved the tool life by 15.5%, 23.6%, 35.5%, and 45.3%, respectively. Under the conditions of cutting parameter 2, compared with the compressed air cooling mode, MQL-R-16, MQL-F-16, MQL-F-32, and MQL-FR-16-16 improved the tool life by 31.6%, 43.6%, 63.9%, and 81.2%, respectively. Obviously, the four MQL modes significantly improved the tool life compared with the compressed air cooling mode. MQL-FR-16-16 had the longest tool life among the four MQL modes.

3.2 Tool Breakage

Because of the particularity of the tool geometry of the solid end mill, a quantitative analysis of tool breakage is much more difficult than with a turning tool. In this study, a quantitative breakage analysis of the solid end mill was realized
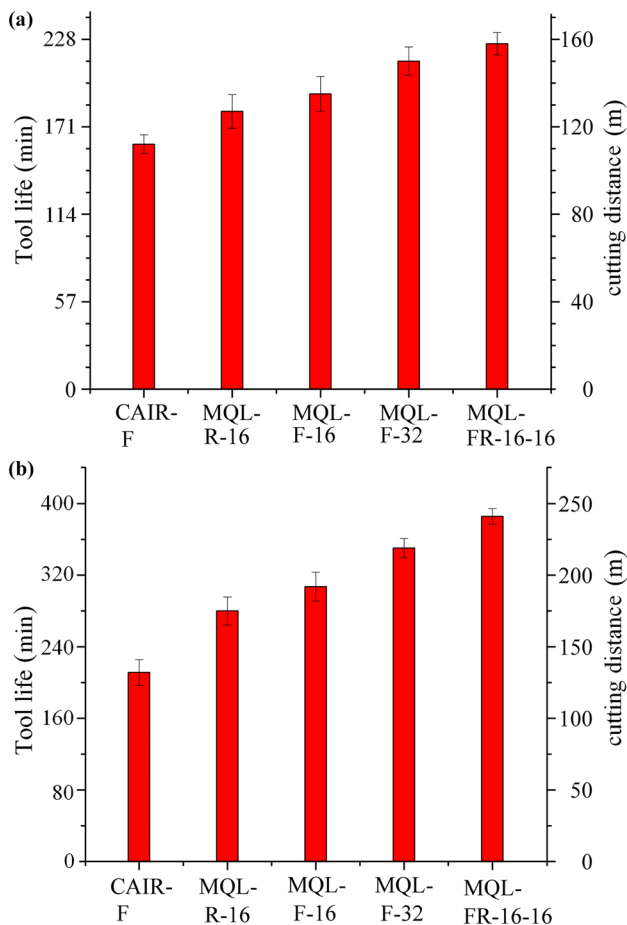

Fig. 4 Comparison of tool life values. **a** Tool life with parameter 1, **b** Tool life with parameter 2

using a precision three-dimensional optical scanner. The results are shown in Fig. 5. Figure 5a shows a cross-section of the 3D model of a worn tool and quantifies the breakage depth of the cutting edge in this section. The cutting edge flank wear of the current section measurement is defined as VB_n, and the cutting edge breakage width value is defined as S_n. Figure 5b and c show the two most severe cutting edges of the MQL-F-16 tool, showing multiple parallel sections at different axial depths and quantifying the tool breakage. Figure 5b and c show that the same cutting edge has different breaking values at different axial depths, and the two cutting edges have different breaking values at the same axial depth position. In turning machining, Sun et al. [26] found that tool wear and tool breakage tended to change synchronously. The tool wear and tool breakage of cutting edge 2 in Fig. 5c generally exhibit a synchronous change, but cutting edge 1 of Fig. 5b does not have this synchronous change correlation. This is related to several factors such as the multiple cutting edges, helical geometry of the cutting edges, and dynamic balance of the rotation. The mean value of tool breakage depth is defined as S, and the mean value of tool flank wear for a cutting tool is defined as VB. Figure 5d and e show analysis results for the S and S/VB values of the tools for the various cutting modes, respectively. As can be seen from Fig. 5d and e, the S and S/VB values are lower for a tool with a slower flank wear process. Obviously, from the point of view of the average, there is still a significant correlation between tool breakage and tool wear.
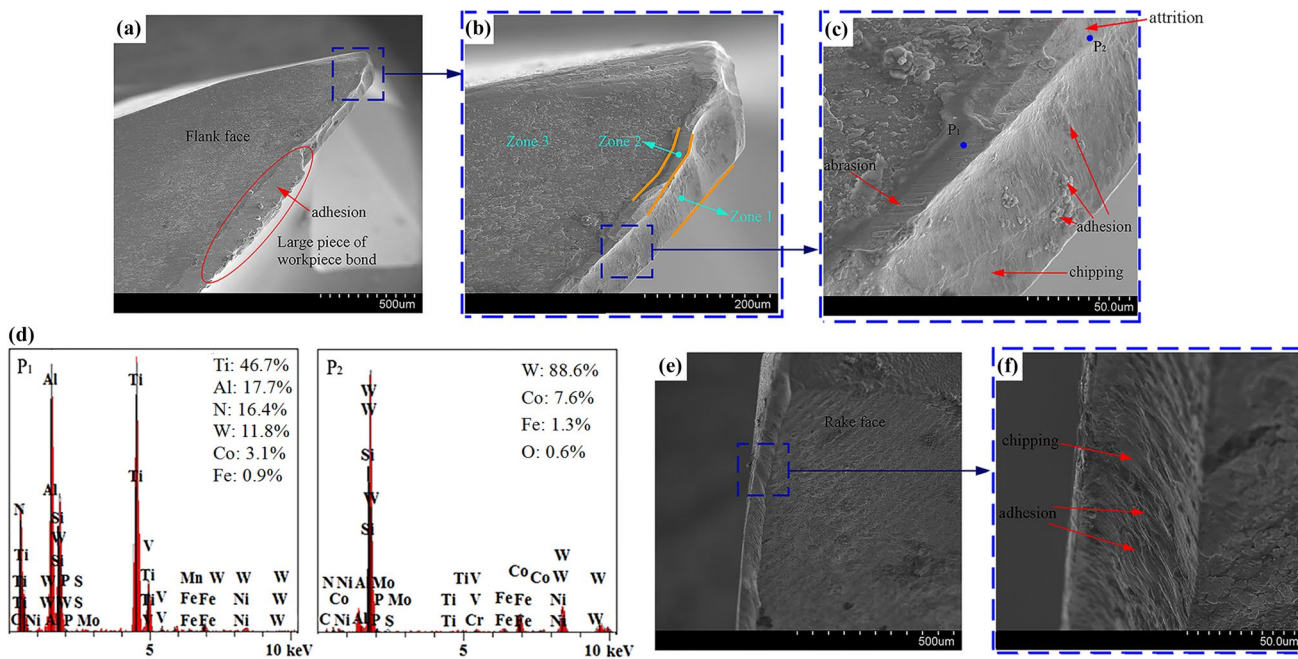
3.3 Microscopic Analysis of Tool

Figure 6 shows scanning electron micrographs of a failed tool after using the compressed air cooling mode. Figure 6a–d are micrographs of the flank wear. In Fig. 6b, the flank face is divided into three main areas. Zones 1 and 2 are flank wear bands. Zone 3 is the area of the flank face that is not worn. Zone 1 is the chipping strip, which is the body of the flank wear strip. Zone 2 can be seen as ridges and grooves parallel to the direction of the cutting speed, which embodies abrasive wear characteristics. Based on an EDS analysis (Fig. 6d), the elements of zone 2 are mainly composed of tool coating elements. A large piece of workpiece bond appears in the flank wear area of Fig. 6a, and significant adhesion of the workpiece material is also visible in the unworn area of Fig. 6b, which reflects the higher cutting temperatures during the cutting process. Figure 6e–f are micrographs of the rake face. There is a chipping strip on the rake face, with some visible bonds, but no obvious abrasion area is seen. The rake face wear is relatively small compared with the flank wear.

Figure 7 shows the microscopic analysis of tool wear for MQL-R-16. Similar to the compressed air cooling mode, the flank face of Fig. 7b clearly identifies three areas. In Fig. 7c,
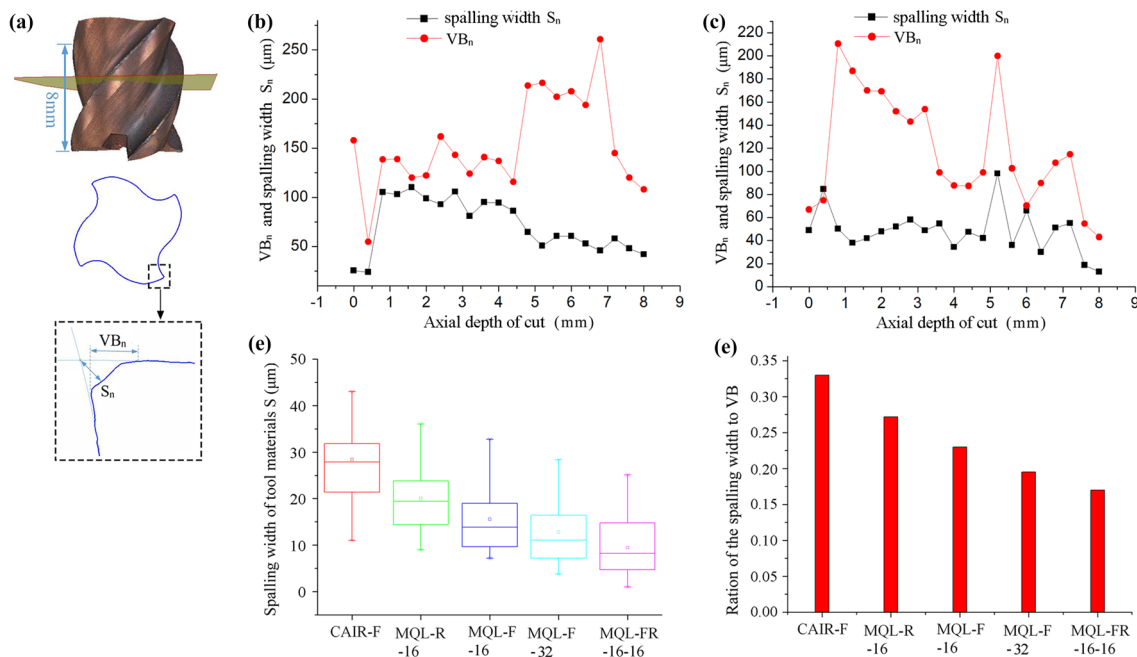
Fig. 5 Quantitative analysis of tool breakage (under parameter 1 cutting conditions). **a** 3D scanning model for cross-section analysis of tool breakage, **b** Quantitative analysis of cutting edge 1 of the MQL-F tool (MQL-F-16, cutting distance 155 m), **c** Quantitative analysis of cutting edge 2 of the MQL-F tool (MQL-F-16, cutting distance 155 m), **d** Comparison of average spalling width of cutting edges (cutting distance 90 m), e. Ratio of average spalling width to mean wear VB (cutting distance 90 m)

Fig. 6 Microscopic analysis of tool wear for CAIR-F (parameter 1). **a** Flank face, **b** Tip area, **c** Partial magnification, d. EDS analysis, **e**, **f** Rake face

there are some adhesion materials in the chipping belt and fresh surfaces formed by the shedding of the adhesion materials. Figure 7d shows that these bonds are workpiece materials. The adhesion of MQL-R-16 is obviously less than that of the compressed gas cooling mode, which indicates that this method can effectively reduce the cutting heat. Zone
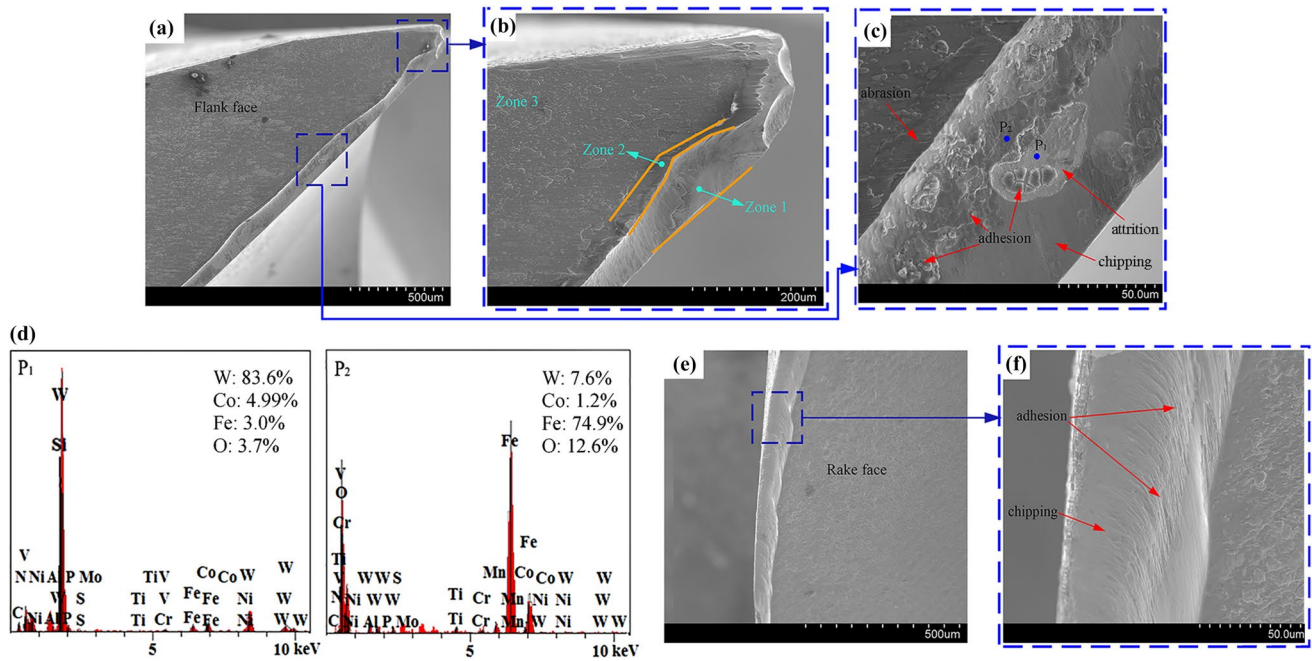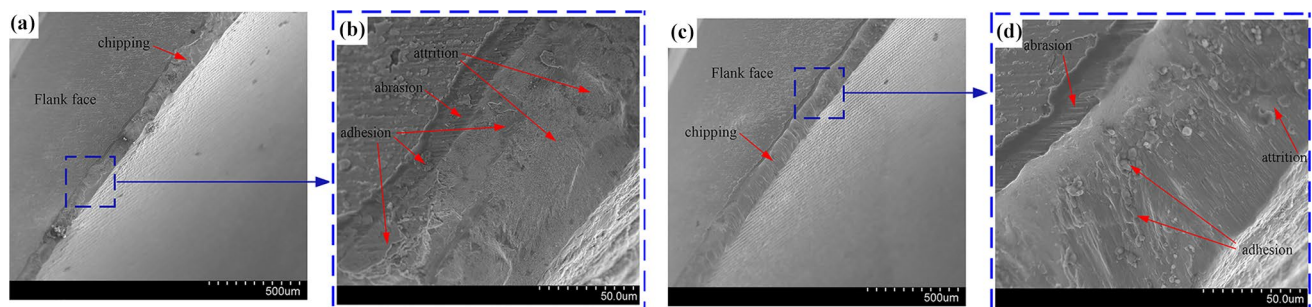
Fig. 7 Microscopic analysis of tool wear for MQL-R-16 (parameter 1). **a** Flank face, **b** Tip area, **c** Partial magnification, **d** EDS analysis, **e**, **f** Rake face

2 in Fig. 7c is the abrasive wear zone and the material composition is primarily the element of tool coating. Figure 7e–f are tool wear micrographs of the rake face. The comparison shows that the rake wear is less than flank wear. The chipping belt zone can be seen on the rake face, but there is no obvious abrasive wear zone.

Figure 8 shows the microscopic analysis of tool wear for MQL-F-16 and MQL-F-32. Some adhesion materials and fresh surfaces formed by the shedding of adhesion materials can also be seen in the chipping belt of MQL-F-16. Compared with MQL-F-16, the adhesion phenomenon in the chipping belt of MQL-F-32 is lighter. Therefore, in the same MQL mode, the increase in the flow rate of the lubricating oil can effectively reduce the thermal wear such as adhesion.
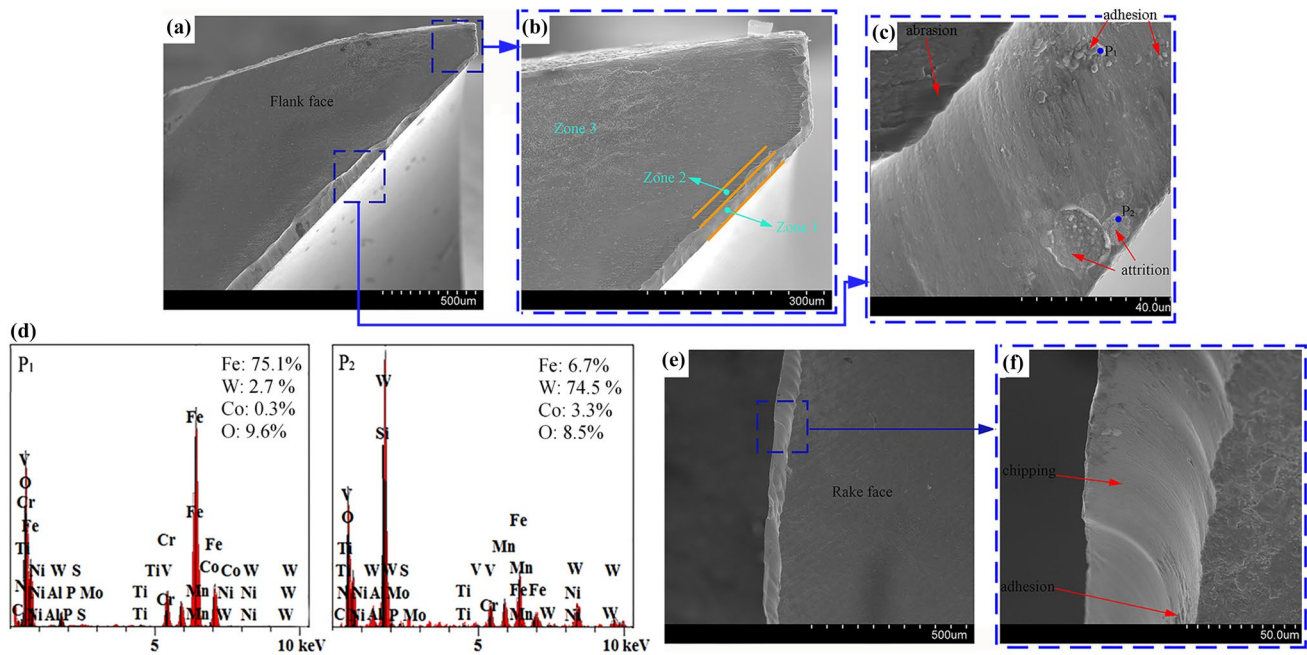
Figure 9 shows the microscopic analysis of tool wear for MQL-FR-16-16. The flank face of Fig. 9b also clearly

identifies three areas. Compared with other MQL modes, MQL-FR-16-16 has the least adhesive materials, indicating that this mode is more effective in reducing the cutting heat and lowering the cutting temperature. In Fig. 9b and c, Zone 2 has distinct grooves and ridges, and the material composition in Zone 2 is primarily the element of tool coating. In Fig. 9c, a small amount of bond cand be seen in the chipping belt and the fresh surface formed by the shedding of bond. Figure 9d shows that these bonds are workpiece materials. Obviously, as the best way of several MQL methods, adhesion is still one of the factors in the development of chipping. Figure 9e and f are micrographs of the rake face. The adhesion phenomenon is relatively slight. As in previous several modes, there is no significant groove and ridge feature on the rake face.
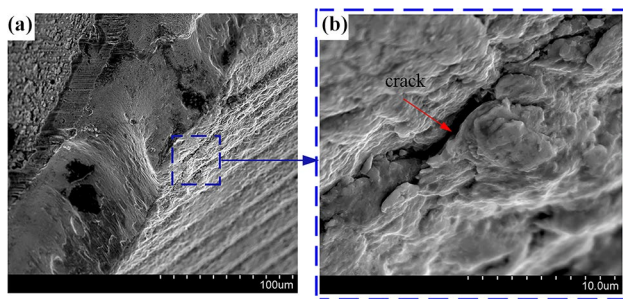

Fig. 8 Microscopic analysis of tool wear for MQL-F-16 and MQL-F-32 (parameter 1). **a**, **b** MQL-F-16, **c**, **d** MQL-F-32

Fig. 9 Microscopic analysis of tool wear in MQL-FR-16-16 (parameter 1). **a** Flank face, **b** Tip area, **c** Ppartial magnification, **d** EDS analysis, **e, f** Rake face

Fig. 10 Microscopic analysis of crack (MQL-F-32). **a** Chipping area and crack, **b** Partial magnification

Figure 10 shows the microcrack of a MQL cutting tool. The microcrack is parallel to the cutting edge direction. This kind of microcrack can be seen in several MQL methods. It is generally believed this kind of microcrack is caused by mechanical load. In the direction perpendicular to the cutting edge, no obvious microcracks were observed in several MQL modes.

3.4 Milling Force

Figure 11 show the evolution of the milling forces in the various cutting modes under parameters 1.

The X-direction effective mean force is defined as F_x, and the Y-direction effective mean force is defined as F_y. The error bar represents the difference between the peak milling force and the effective mean milling force. As the cutting distance increases, the F_x curve changes gently, which should be related to the spalling of the cutting edge material during the cutting process. As the cutting distance increases, the F_y values of the cutting modes increase significantly. In the middle and late stages of cutting, the Y-direction force F_y is significantly larger than the X-direction force F_x.

The resultant force is defined as F. It can be calculated using the following formula:

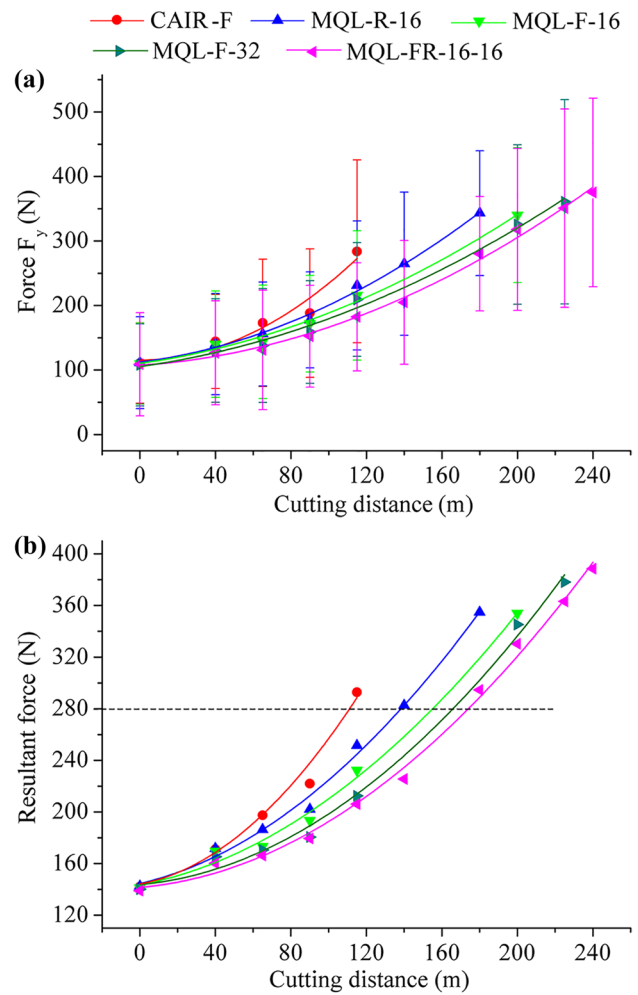$$F = \sqrt{F_x^2 + F_y^2}. \tag{1}$$

In Fig. 11, the F_y curve graphs of the cutting modes are close to the F curve graphs, indicating that F_y is the main part of the resultant force. Figure 12 is the milling diagram under parameter 2. Similar to Fig. 11, F_y is the main part of the resultant force.

As can be seen from Figs. 11 and 12, the steepness values of the resultant force F curves of CAIR-F, MQL-R-16, MQL-F-16, and MQL-FR-16-16 sequentially decrease. In Fig. 11, when the resultant force reaches 350 N, the cutting distances of the cutting modes are 100 m, 117 m, 131 m, 143 m and 154 m in turn. In Fig. 12, when the resultant force reaches 280 N, the cutting distances of the various modes are 111 m, 138 m, 154 m, 165 m and 175 m in turn. By comparing the resultant force curve with the tool wear curve (Fig. 3), it can be found that they have a corresponding relationship, with a faster tool wear associated with a greater increase in the milling force.
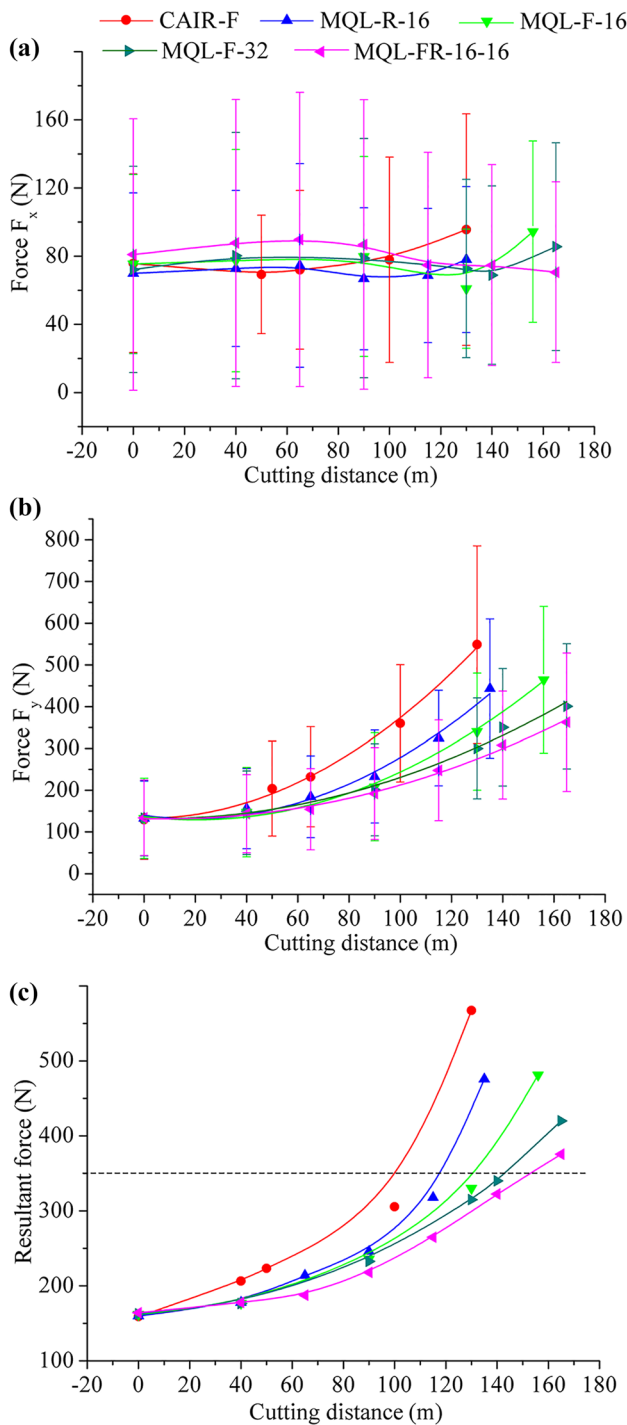
Fig. 11 Milling force evolution curve under parameter 1. **a** F_x, **b** F_y, **c** Resultant force F

Fig. 12 Milling force evolution curve under parameter 2. **a** F_x, **b** F_y, **c** Resultant force F

less adhesion and storage of lubricating oil. When cutting a certain distance, the lubricating action of the lubricating oil gradually becomes obvious, and the difference between the tool wear and cutting force gradually increases. This should be related to some scratch marks in the rake face and flank face. These groove scratches enhance the ability of the surface to adhere and store the oil film, and provide some micro-channels for the penetration of the lubricating oil into the cutting contact area [27].

3.5 Chips

Figure 13 shows the chip evolution processes for the various cutting modes. The chips of the compressed air cooling mode reach a flat shape within the range of 70–90 m. The chips of MQL-R-16 reach a flat shape at 130 m. The flatness of the chip shows that the cutting edge has been passivated. The chips of MQL-F-16 are still relatively curled at 130 m, but the chip length is significantly

It can also be seen from Fig. 11 that at the beginning of the cutting, the lubricating action of the lubricating oil is not obvious, and the F_y milling forces (or F resultant forces) of the MQL modes are close in magnitude. Figure 12 has a similar result. This may be because the surface roughness of the cutting edge is low in the initial stage of cutting, resulting in
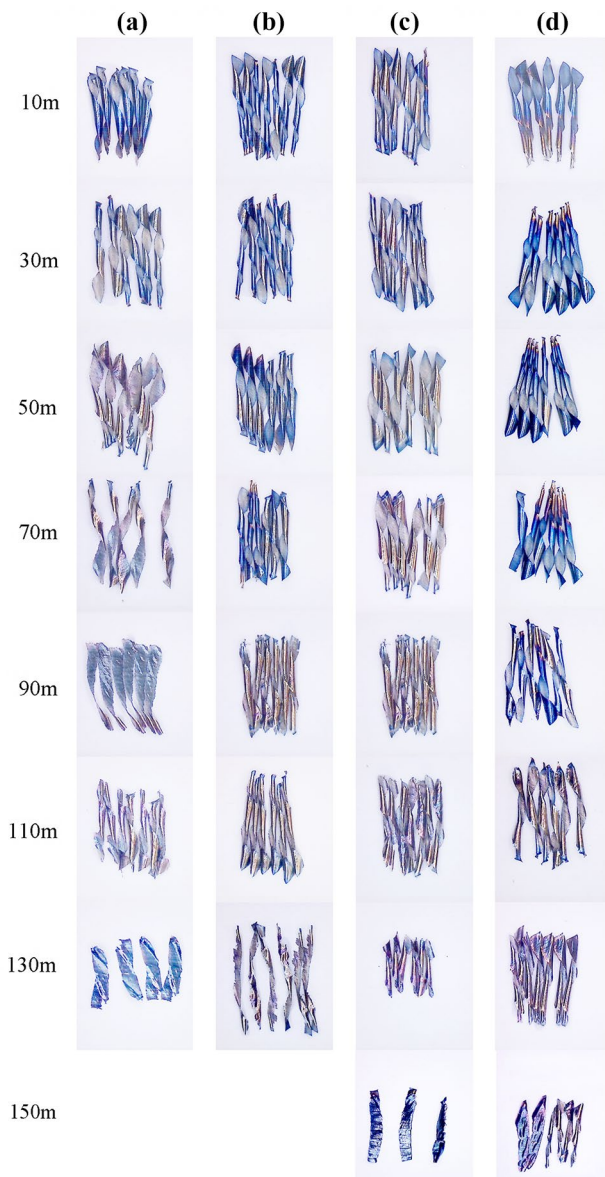
Fig. 13 Chip evolution process (parameter 1). **a** CAIR-F, **b** MQL-R-16, **c** MQL-F-16, **d** MQL-FR-16-16

Fig. 14 Comparison of chip curvatures of four cutting modes under parameter 1. (To make the diagram more intuitive, the curvature value of flat state chips is represented by the value 900 μm with an upward arrow, but the actual curvature value exceeds 3000 μm)

reduced, which is related to some local chipping. The chips of MQL-FR-16-16 maintain good curls from 0 to 130 m. Obviously, the chip evolution reflects the tool wear process. When the cutting edge wears lightly, the chip curls significantly and the chips are long. Thereafter, the cutting edge wears and some chipping occurs, at which time the chips are curled but become shorter. As more chipping occurs and engages, the cutting edges passivate, and the chips no longer curl, but become flat. Further, the chips of the CAIR-F mode in Fig. 13 undergo a "curl-flat-crimp-re-flat" transition process from 70 to 110 m. Similar phenomena may be seen in several other ways during the middle and late stages of cutting, indicating that the cutting edge

has a "self-sharpening" phenomenon. The phenomenon of "self-sharpening" is more common in grinding, but there are a few related reports on solid end mills in the literature. The self-sharpening of the milling cutter may be related to the further peeling of the rake face and flank face after the cutting edge is passivated. This peeling will, to some extent, sharpen the passivated cutting edge again.

Chip curvatures of the various cutting modes were analyzed statistically. The result is shown in Fig. 14. At a cutting distance of 20 to 100 m, the chip curvature is relatively stable. The curvature radius of the chip in several ways in this interval can be roughly sorted as: CAIR-F > MQL-F > MQL-FR > MQL-R. The possibility of causing the above curvature results may be related to the lubrication of rake face. Due to the lack of oil fog lubrication, the chip curvature of the compressed air cooling mode is the largest. The nozzle of the MQL-F mode mainly sprays the flank face of the cutting edge, and only a small amount of lubricating oil is sprayed on the rake face during the empty cutting stage. Both the MQL-R and MQL-FR modes can effectively spray the rake face of cutting edge for effective lubrication. Since the air pressure and flow rate in the MQL-FR mode are slightly lower than MQL-R, the lubrication effect of the MQL-FR mode on the rake face should be slightly lower than that of the MQL-R mode. Therefore, the lubrication effect of several cutting modes on the rake face should be: CAIR-F < MQL-F < MQL-FR < MQL-R. Based on the above analysis, an effective conclusion can be drawn basically. The better the lubrication effect on rake face, the smaller the chip curvature. The discussion of lubrication and chip curvature will be further analyzed in the later discussion section.

4 Discussion

4.1 Tool Wear and Breakage Mechanism

Tool wear is closely related to the cutting costs and surface quality of a machined workpiece. During the high-speed milling of hardened steel, the tool wears quickly, accompanied by the peeling and tearing of the tool material. In order to explain the tool wear and breakage mechanism, it is necessary to analyze the stress state of the cutting edge during high-speed milling first.

Figure 15 shows the basic geometry of milling. With tool radius r and radial depth of cut Ae, the engagement angle θ_m can be calculated using the following formula:

$$\theta_m = arcos((r - A_e)/r). \tag{2}$$

During the milling process, the instantaneous milling thickness (h) of each cutting edge can be calculated using formula (3):

$$h(\theta) = f \sin \theta, \tag{3}$$

where f is the feed per tooth, and θ is the rotation angle.

For each cutting edge, the average cutting material thickness per revolution is as follows:

$$h_a = \left| \int_0^{\theta_m} f \sin \theta d\theta \right| \Big/ \theta_m. \tag{4}$$

Based on the values of cutting parameter 1 listed in Table 1, $\theta_m = 28.95°$ and $h_a = 6.2$ μm can be calculated. Based on the engagement angle of the cutting edge fully cut into the workpiece ($\theta_m = 28.95°$) and the spiral lag angle ($\pi/4$), the axial depth of cut can be calculated to be 2.02 mm. Referring to the cutting force of Fig. 11, the mean stress of the cutting edge during the initial cutting process can be approximately computed to be 12.8 GPa (160 N/(6.2 μm × 2.02 mm) = 12.8 GPa). The working stress of 12.8 GPa is significantly greater than the ultimate tensile stress (3.2 GPa) of cemented carbide [28]. When the cutting edge has wear characteristics such as adhesion and chipping, the local stress of the cutting edge will be much greater than 12.8 GPa.

According to the above calculations, the cutting edge is subject to intermittent high cutting stress during the high-speed milling of hardened steel, which may cause several consequences: (1) the cutting edge is prone to plastic deformation, (2) high-frequency impact causes fatigue, (3) the friction is large, (4) the cutting temperature is high, and (5) adhesion and seizure can easily occur. Understanding these characteristics is necessary to understand the mechanism of tool wear and tool breakage.

As mentioned in Sect. 3.3, the wear characteristics of the rake face are mainly adhesion/attrition wear and flaking/chipping. The main wear characteristics of the flank face are abrasion wear, adhesion/attrition wear, and flaking/chipping. Both the compressed air cooling and MQL modes showed the above wear characteristics, with varying degrees of severity.

Abrasion grooves parallel to the cutting direction occurred at the flank faces of each cutting stage in the compressed air cooling and MQL methods. Abrasion is more critical in flank wear, because the tool flank rubs against a rigid element (workpiece), whereas the contact between the tool rake face and chip involves sliding and seizure [29]. Whether the abrasive particles are harder or softer than the
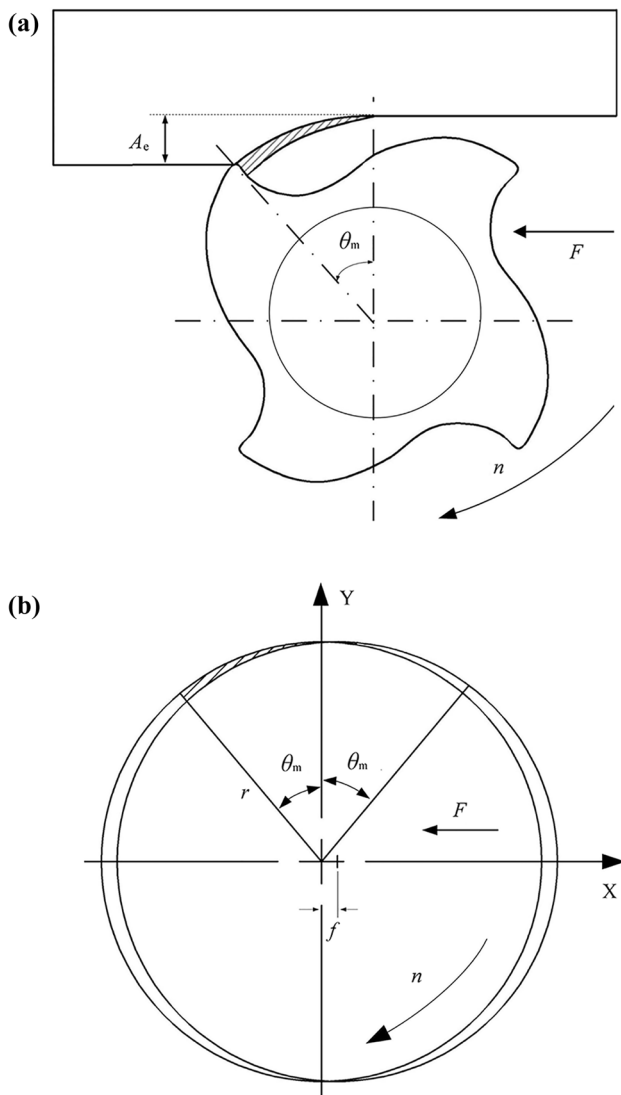
Fig. 15 Schematic diagram of tool cutting. **a** Cutting contact process, **b** Basic geometric relation

surface, an abrasion phenomenon can be produced, and the abrasion can be divided into hard and soft abrasion [30]. Hardened steel containing the martensite phase is a hard and difficult-to-work material. Under high cutting friction stress conditions, it is easy to generate abrasion wear on a cemented carbide tool (Figs. 6, 7, 8, and 9). If hard particles of the tool, coating, and chip debris enter the area between the workpiece and flank face, more contact stress occurs, which further promotes abrasion wear.

The adhesion or welding of the workpiece material can be observed on the flank and rake faces of the tool. Because the adhesion materials are not stable, they may break off, along with a small lump of tool particles. This phenomenon is called attrition. Different levels of adhesion/attrition were found in the compressed air cooling mode and MQL modes. The thermal softening of workpiece materials caused by the higher temperature and higher stresses has been found to be the main reason for the adhesion of the workpiece material [31]. As previously mentioned, the high-speed milling conditions for hardened steel produce high cutting stresses, and cause high friction and high cutting temperatures, which create good conditions for the formation of adhesion. Adhesion is an important indicator of the severity of tool wear/breakage. Because of the lack of sufficient cooling and lubrication in the compressed air cooling mode, obvious workpiece bonding and pits where the bond peeled off could be seen on the cutting edges, with even a large piece of adhesive material seen in the later stage of cutting. By lubricating the cutting area with an oil mist, MQL reduced the cutting friction, cutting stress, and cutting temperature, and thus relieved the adhesion phenomenon, with a better cooling/lubrication effect resulting in a lighter degree of adhesion/attrition. The MQL-FR-16-16 method had the lighter degree of adhesion/attrition of the four MQL modes at each stage, showing that it had the best cooling/lubricating effect.

Chipping/flaking was another major tool wear/breakage feature of the compressed air cooling mode and MQL modes. The chipping/flaking bandwidth of the flank face was larger than that of rake face. Because the chipping/flaking belt occupied the main body in the wear belt, the chipping/flaking wear mechanism was the key to understanding the tool wear and tool breakage mechanism in high-speed milling with solid end mills. Based on previous research results, the formation of chipping may be related to abrasion, adhesion/attrition [32, 33], mechanical shock and cracking [34], and thermal fatigue [32, 35]. These four aspects will be analyzed one by one. The compressed gas air-cooling and MQL modes showed abrasion areas with grooves and ridges in the flank face. The material found in this area was mainly composed of the tool coating. Therefore, abrasion could be seen as a prelude to the formation of chipping. When the tool coating and superficial layer of the substrate were subjected to abrasion to a certain extent, the underlying tool base began to be exposed and further peeled

off, and the width of the chipping belt increased. The different MQL methods showed the adhesion/attrition phenomenon to different degrees at each cutting stage. The frequent occurrence of adhesion/attrition removed a portion of the cemented carbide matrix particles and promoted the development of chipping. Thermal fatigue could be excluded because no thermal cracks were found perpendicular to the cutting edge with the MQL methods. Mechanical cracks (Fig. 10) parallel to the cutting edge could be found in the MQL modes, which were mainly caused by mechanical shock. During the high-speed milling of hardened steel, the cutting edge is subjected to intermittent high cutting stress, which is significantly greater than the ultimate tensile stress of the cemented carbide. Fatigue occurs as the result of the intermittent high cutting impact forces. Then, mechanical cracking may occur and induce local chipping or flaking in a cemented carbide tool with brittle characteristics. In addition, solid end mills have different amounts of cutting edge breakage at different axial depths (Figs. 5b and c). In other words, a portion of the cutting edge is relatively "convex." The local "convex" portion of the cutting edge is clearly subject to greater concentrated stress [36], far exceeding the ultimate stress of the tool material. Thus, these "bulge" portions are more prone to local chipping. Based on the above analysis, abrasion, adhesion/attrition, intermittent mechanical shock, and cracking are the main mechanisms in the formation of chipping/flaking.

The quantitative analysis presented in Sect. 3.2 showed that there is a significant correlation between tool breakage and tool wear. The main body of the tool wear area is the chipping/flaking belt. Therefore, the formation and development mechanism of tool breakage should be the same as that of chipping/flaking.

The MQL methods were effective at reducing the tool wear and breakage compared with the compressed air cooling method. The oil mist could enter the second deformation zone between the rake face and chips, or the third deformation zone between the flank face and workpiece. This resulted in two major changes. First, the friction decreased, along with the frictional power. Second, the cutting force decreased, which led to a decrease in the cutting stress. These two changes could effectively inhibit the abrasion, adhesion, mechanical cracking, chipping/flaking, etc. The MQL-FR-16-16 method could provide effective boundary lubrication for both the rake face and flank face. Compared with the other MQL methods, it produced more benign changes in reducing the stress, friction, and temperature. Thus, the tool wear and breakage process was the lowest.

4.2 Spraying Models

MQL uses different injection methods to produce different processing effects. Through geometric analysis, the injection model shown in Fig. 16 could be established.

The injection model of MQL-F is shown in Fig. 16a. The jet flow is in the same direction as the cutting edge cut into the workpiece. The Y + axis is specified as 0°, and the clockwise rotation angle is positive. The tool rotation could be divided into three stages: empty cut stage I (0°–270°), empty cut stage II (270°–θ, when $A_p = 0.5$ mm, then $\theta = 334$°), and cutting material stage III (θ–360°). In the first stage, the tool rotates and is air cooled; in the second stage, as the tool rotates, the jet flow is first sprayed on the rake face and then
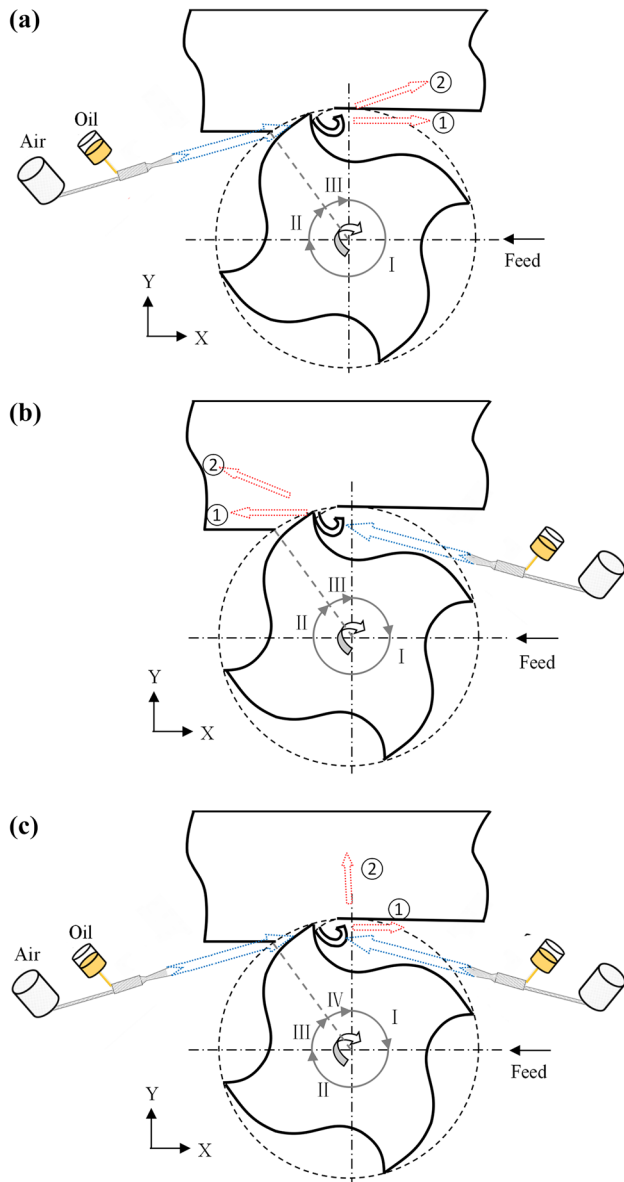
Fig. 16 Injection models of three MQL cutting modes. **a** MQL-F, **b** MQL-R, **c** MQL-FR. (Arrow ① represents the direction of jet traction during the upward growth of the chip from the bottom layer to the surface layer of the workpiece. In the direction of traction, arrow ② represents the direction in which chips are grown upward to a certain extent beyond the surface of the workpiece by the jet traction force)

on the flank face of the cutting edge. The compressed gas applies cooling to the cutting edge, and the carried trace oil can also adhere to the rake face and flank face and provide surface lubrication for the third stage. In the third stage, the jet flow is mainly sprayed on the flank face of the cutting edge, which is thus cooled and lubricated. Because of the geometric characteristics of the helical lag angle of the cutting edge, the jet flow can blow away the upward growing chip and prevent it from making full contact with the rake face (see arrows ① and ② in Fig. 16a), which prevents the chip heat from remaining and entering the rake face, and prevents the chip from being cut again. Because of the lubrication effect of the second and third stages, the tool wear condition of the MQL-F mode is significantly lower than that of the compressed air cooling mode.

The injection model of MQL-R is shown in Fig. 16b. The jet flow is in the opposite direction as the cutting edge cut into the workpiece. The tool rotation could be divided into three stages: empty cut stage I (0°–90°), empty cut stage II (about 90°–θ, when $A_p = 0.5$ mm, then $\theta = 334$°), cutting material stage III (θ–360°). In the first stage, as the tool rotates, the jet flow is first sprayed on the rake face and then on the flank face of the cutting edge. The compressed gas cools the cutting edge, and a small amount of lubricating oil can adhere to the blade surface to form a lubricating oil film. In the second stage, the tool rotates and is air cooled. In the third stage, the jet flow is primarily sprayed onto the rake face of the cutting edge. According to the analysis of tool wear (Sect. 3.1) and chip curvature (Sect. 3.5), the MQL-R oil mist jet can effectively intervene in the rake face-chip contact area to apply lubrication. However, the lubrication effect of MQL-R on the cutting zone is weaker than that of the MQL-F mode, which can be drawn from the comparison of their tool wear curves (Fig. 3). Three reasons cause the MQL-R tool to wear faster than the MQL-F mode. Firstly, in the process of the chip growth in the MQL-R mode from the bottom up, the jet flow has certain suppression effect on the chip growth (see the drawing arrow directions ① and ②), and the chips may be cut twice. Secondly, part of the MQL-R jet flows are easily blocked by the non-cutting edge (Fig. 16b). Thirdly, the MQL-R jet usually cannot fully direct the cutting contact area between the rake face and the chip, because the cutting edge rotates to the right at the same time during the chip curling process (Fig. 16b).

The injection model of MQL-FR is shown in Fig. 16c. Tool rotation is divided into four stages: empty cut stage I (0°–90°), empty cut stage II (about 90°–270°), and empty cut stage III (about 270° − θ, when $A_p = 0.5$ mm, then $\theta = 334$°), and cutting material stage IV (θ–360°). In the first and third stages, as the tool rotates, the jet flow is first sprayed on the rake face and then on the flank face of the cutting edge. The compressed gas cools the cutting edge, and the traced lubricating oil droplets can adhere to the rake face and flank

face to form oil films. In the second stage, the tool rotates and is air cooled. In the fourth stage, the F-direction jet can be effectively injected into the cutting contact zone between the rake face and the chip (Sect. 3.5), and the R-direction jet can be effectively injected into the contact zone between the flank face and workpiece. Since two jets can effectively lubricate the rake face and flank face of the cutting edge, the tool wear of MQL-FR is significantly lower than that of MQL-F and MQL-R. In addition, the direction of jet traction during the upward growth of the chips is indicated by arrows ① and ② of Fig. 16c, which indicates that the chips do not excessively contact the rake face to conduct heat, and the chips are not easily cut again.

4.3 Cooling and Lubricating Mechanism

MQL has the effect of cooling and lubrication. It is generally believed that the cooling effect of MQL is limited [37–39], and lubrication is the main mode of action of MQL. Based on the oil mist lubrication characteristics, the force, heat, and friction wear in MQL cutting were quantitatively analyzed during two-dimensional orthogonal cutting.

Figure 17 shows the MQL two-dimensional orthogonal cutting model. Figure 17a shows an MQL injection model. In the MQL-F mode, the air jet is sprayed toward the tool flank face by a single nozzle. In the MQL-R mode, the air jet is sprayed toward the tool rake face by a single nozzle. In the MQL-FR mode, double nozzles respectively spray air jets toward the rake face and flank face of the tool. In these MQL modes, a certain amount of oil mist is sprayed and adhered to the rake and flank faces at the empty stage (see Sect. 4.2). Figure 17b shows a cutting foundation model that includes the cutting component and resultant force of the first and second deformation zones. The MQL oil mist provides boundary lubrication that changes the cutting friction and cutting force state.

The given shear stress in the shear plane is defined as τ_s; the chip thickness ratio is r_c; the shear strain is γ; the chip width is b; the specific shear energy is μ_s; and the specific friction energy in the second deformation region is $\mu_{f\text{-}R}$. According to Rao [40], the resultant force and shear strain have the following relationship:

$$R = \tau_s b t_1 / \sin \varphi \cos(\varphi + \beta - \alpha). \tag{5}$$

The unit cutting energy has the following relationship:

$$\mu = \mu_s + u_{f-R} = \tau_s \gamma + F r_c / b t_0 = \tau_s \gamma + (R \sin \beta)/b t_c. \tag{6}$$

Merchant [41], and Lee and Shaffer [42] respectively derived the following two relations:
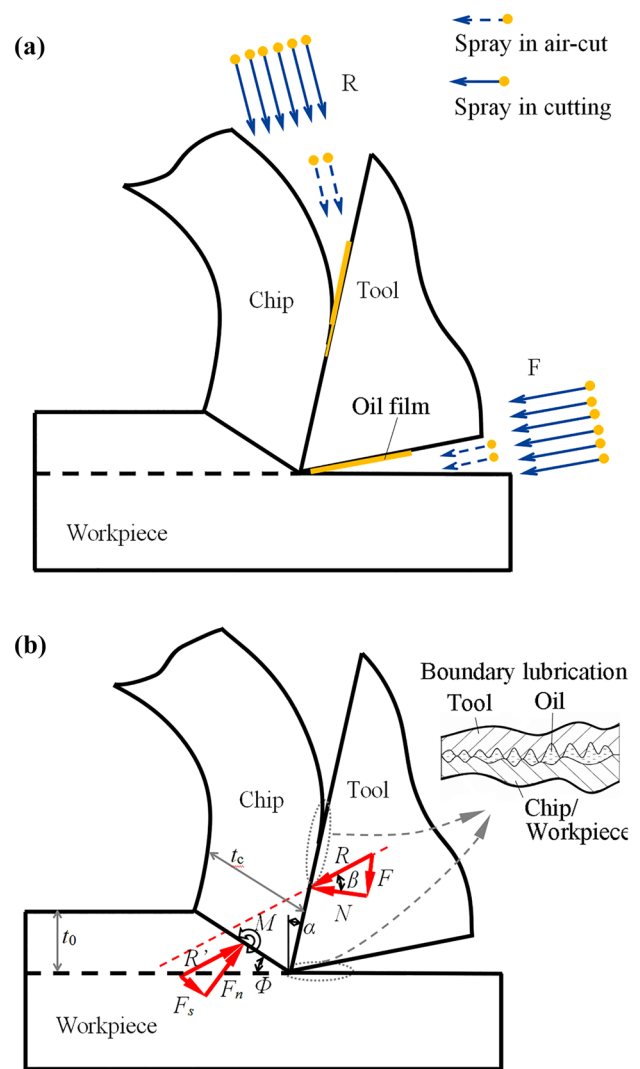
$$\varphi = \pi/4 + (\alpha - \beta), \tag{7}$$

Fig. 17 Orthogonal cutting model in MQL environment. **a** Injection model, **b** Cutting model

$$\varphi = \pi/4 + (\alpha - \beta)/2. \tag{8}$$

When the compressed gas carries the atomized oil droplets into the cutting contact area between the tool and chip (Fig. 17b) to form a boundary lubrication film, the tool–chip friction can be reduced, that is, friction angle β is reduced [16]. According to Eqs. 7 and 8, after friction angle β is decreased, shear angle $\varPhi$ is correspondingly increased. Based on Eqs. 7 and 8, it is generally known that $|d\beta| > |d\varPhi|$. Therefore, in Eq. 5, if the shear stress in the shear plane τ_s is constant, the resultant force R will decrease. The frictional resistance F ($F = R\sin\beta$) of the chip flow also decreases accordingly. Under the usual rake angle condition, if the shear angle is increased, shear strain γ generally decreases. In addition, it is clearly established that $|d(R\sin\beta)| > |dt_c|$ or $|dF| > |dt_c|$. Therefore, when the tool–chip friction decreases,

the total unit cutting energy of Eq. 6 decreases, along with the cutting force, cutting contact stress, and cutting heat. Correspondingly, the mechanical impact, adhesion, and other wear factors are effectively reduced. The MQL-R and MQL-FR modes are superior to the compressed air cooling mode, which provides strong evidence for the above analysis results. Compared with the compressed air cooling method, the MQL-R and MQL-FR modes significantly slow down the evolution processes for the tool wear and cutting force, precisely because both of these methods provide very effective lubrication for the rake face–chip contact area.

Equation 6 is suitable when the flank wear is small. With the progress of cutting, the wear between the flank face and workpiece cannot be ignored. Thus, Eq. 6 should also increase the friction energy $\mu_{f\text{-}F}$ between the flank face and workpiece. Because the formula for calculating the friction energy between the flank face and workpiece has some complexity, this paper does not present all of the details. Only the qualitative analysis formula is given below.

$$\mu = \mu_s + u_{f-R} + u_{f-F}. \tag{9}$$

When the MQL jet is injected into the cutting contact area between the tool and workpiece (Fig. 17b), it is also possible to form a boundary lubrication film, which reduces the friction energy $\mu_{f\text{-}F}$ between the tool and workpiece, and also reduces the shear energy μ_s. Therefore, the total unit cutting energy μ of Eq. 9 decreases, along with the cutting force, cutting contact stress, and cutting heat. These changes will effectively suppress the tool wear, including mechanical cracking, adhesion, and chipping. Both the MQL-F and MQL-FR modes can lubricate the flank face. Compared with the compressed gas air cooling method, the tool wear and cutting force evolution processes are significantly reduced, which provide evidence for the above analysis results.

Increasing the lubricating oil flow rate can enhance the tool–chip and tool–workpiece boundary lubrication effects, further decreasing the cutting friction and total unit cutting energy, and thus effectively decreasing the cutting contact stress, temperature, adhesion, and mechanical impact so as to slow down the process of tool wear. Compared with MQL-F-16 and MQL-R-16, the tool life with MQL-FR-16-16 and MQL-F-32 is significantly improved, which strongly illustrates the importance of the lubricating oil flow rate. Increasing the oil flow rate will also bring environmental pollution risks. The oil flow rate used in this study was controlled to a small value.

Under the same lubricating oil flow rate conditions, the double nozzle mode of simultaneously spraying jets at the rake face and flank face was superior to the single nozzle mode of spraying only a single face of the cutting edge. MQL-FR-16-16 significantly prolonged the tool life under both sets of cutting parameters compared with MQL-F-32.

The fundamental reason was that the lubricating oil mist simultaneously sprayed the second and third deformation zones, which could reduce the total unit cutting energy, cutting contact stress, cutting heat, and cutting temperature more effectively than spraying a deformation zone separately.

In addition to reducing the tool–chip friction, cutting heat, and cutting force, the oil mist sprayed on the rake face could also change the chip curvature and other characteristics. An analysis of this is presented as follows. The positive pressure N and frictional force F on rake face form a resultant force R, and the positive pressure F_n and shear force F_s on the shear plane form a resultant force R'. Normally, these two resultant forces are assumed to be equal in magnitude and opposite in direction to facilitate some basic calculations. However, in reality, the combined forces of R and R' are generally not collinear. They form a bending moment M that will cause chip curling [43]. Based on this mechanism, the friction on the rake face essentially prevents a chip from curling. In other words, if the chip flow friction is decreased, the degree of chip curling should be increased (the curl radius will be correspondingly decreased). The lubrication effects of MQL-FR-16-16 and MQL-R-16 on the rake face were significantly better than those of MQL-F-16 and CARI-F. At a stable cutting stage, the chip curl curvatures of MQL-FR-16-16 and MQL-R-16 were significantly less than those of MQL-F-16 and CARI-F (Fig. 14), which provided very strong evidence for the above analysis results. Compared with the other two methods, MQL-FR-16-16 and MQL-R-16 could spray the oil mist onto the rake face and so could effectively reduce chip the flow resistance, thus resulting in a reduction in the chip curl curvature.

5 Conclusions

This study investigated the use of MQL in the high-speed milling of hardened steel using a carbide solid end mill. The conclusions are as follows:

(1) The milling force and tool wear values were successively reduced using MQL-F, MQL-R, MQL-F, and MQL-FR. Among these, MQL-FR as the optimal cooling and lubrication mode could effectively reduce the cutting contact stress and unit cutting energy, and significantly reduce wear phenomena such as adhesion and chipping.

(2) In the MQL environment, the wear characteristics of the rake face of a solid end mill were mainly adhesion/attrition wear and flaking/chipping. The main wear characteristics of the flank face were abrasion wear, adhesion/attrition wear, and flaking/chipping. Abrasion, adhesion/attrition and mechanical shock were the

main mechanisms causing chipping/flaking in the solid end mill. A clear correlation existed between the tool breakage and tool wear. The development of chipping/flaking was accompanied by tool breakage, and the tool breakage mechanism was the same as that of chipping/flaking.

(3) Lubrication had a great influence on cutting performance. The lubrication mechanism during the high-speed milling using the solid end mill consisted of an oil mist injected into the tool–chip and tool–workpiece cutting contact areas; the reduction of the tool–chip and tool–work friction, total unit cutting energy, cutting contact stress, heat, and temperature; and ultimately the reduction of the abrasive wear, adhesion, and chipping.

(4) The curvature radius of the chip was an important indication of the lubrication condition of the rake face, with a better lubrication effect on the cutting contact area between the rake face and chip producing chips with a smaller curl curvature radius.

Compliance with ethical standards

Conflict of interest The authors declare that they have no conflict of interest.

References

1. Wu, S. X., Ma, W., Li, B., & Wang, C. Y. (2016). Trochoidal machining for the high-speed milling of pockets. *Journal of Materials Processing Technology, 233*, 29–43.

2. Wu, S. X., Li, Z. Y., Wang, C. Y., Li, S. Y., & Ma, W. (2018). Tool wear of corner continuous milling in deep machining of hardened steel pocket. *International Journal of Advanced Manufacturing Technology, 97*(1–4), 1315–1333.

3. Pervaiz, S., Anwar, S., Qureshi, I., & Ahmed, N. (2019). Recent advances in the machining of titanium alloys using minimum quantity lubrication (MQL) based techniques. *International Journal of Precision Engineering and Manufacturing-Green Technology, 6*(1), 133–145.

4. Weinert, K., Inasaki, I., Sutherland, J. W., & Wakabayashi, T. (2004). Dry machining and minimum quantity lubrication. *CIRP Annals-Manufacturing Technology, 53*(2), 511–537.

5. Paul, S., Dhar, N. R., & Chattopadhyay, A. B. (2001). Beneficial effects of cryogenic cooling over dry and wet machining on tool wear and surface finish in turning AISI 1060 steel. *Journal of Materials Processing Technology, 116*(1), 44–48.

6. Sen, B., Mia, M., Krolczyk, G., Mandal, U. K., & Mondal, S. P. (2019). Eco-friendly cutting fluids in minimum quantity lubrication assisted machining: a review on the perception of sustainable manufacturing. *International Journal of Precision Engineering and Manufacturing-Green Technology*, 1–32.

7. Wang, C. Y., Xie, Y. X., Qin, Z., Lin, H. S., Yuan, Y. H., & Wang, Q. M. (2015). Wear and breakage of TiAlN- and TiSiN-coated carbide tools during high-speed milling of hardened steel. *Wear, 336–337*, 29–42.

8. Sun, S., Brandt, M., & Dargusch, M. S. (2010). Machining Ti-6Al-4V alloy with cryogenic compressed air cooling. *International Journal of Machine Tools and Manufacture, 50*(11), 933–942.

9. Cai, C. Y., Liang, X., An, Q. L., Tao, Z. R., Ming, W. W., & Chen, M. (2020). Cooling/Lubrication performance of dry and supercritical CO₂-based minimum quantity lubrication in peripheral milling Ti-6Al-4V. *International Journal of Precision Engineering and Manufacturing-Green Technology*. https://doi.org/10.1007/s40684-020-00194-7.

10. Musfirah, A. H., Ghani, J. A., & Haron, C. H. C. (2017). Tool wear and surface integrity of Inconel 718 in dry and cryogenic coolant at high cutting speed. *Wear, 376–377*, 125–133.

11. Pereira, O., Rodríguez, A., Barreiro, J., Fernández-Abia, A. I., & De Lacalle, L. N. L. (2017). Nozzle design for combined use of MQL and cryogenic gas in machining. *International Journal of Precision Engineering and Manufacturing-Green Technology, 4*(1), 87–95.

12. Masoudi, S., Esfahani, M. J., Jafarian, F., & Mirsoleimani, S. A. (2019). Comparison the effect of MQL, wet and dry turning on surface topography, cylindricity tolerance and sustainability. *International Journal of Precision Engineering and Manufacturing-Green Technology, 6*(2), 100–113.

13. Dureja, J. S., Singh, R., Singh, T., Singh, P., Dogra, M., & Bhatti, M. S. (2015). Performance evaluation of coated carbide tool in machining of stainless steel (AISI 202) under minimum quantity lubrication (MQL). *International Journal of Precision Engineering and Manufacturing-Green Technology, 2*(2), 123–129.

14. Sreejith, P. S. (2006). Machining of 6061 aluminium alloy with MQL, dry and flooded lubricant conditions. *Materials Letters, 62*(2), 276–278.

15. Tawakoli, T., Hadad, M. J., & Sadeghi, M. H. (2010). Influence of oil mist parameters on minimum quantity lubrication-MQL grinding process. *International Journal of Machine Tools and Manufacture, 50*(6), 521–531.

16. Rahim, E. A., & Sasahara, H. (2011). A study of the effect of palm oil as MQL lubricant on high speed drilling of titanium alloys. *Tribology International, 44*(3), 309–317.

17. Zhang, S., Li, J. F., & Wang, Y. W. (2012). Tool life and cutting forces in end milling Inconel 718 under dry and minimum quantity cooling lubrication cutting conditions. *Journal of Cleaner Production, 32*, 81–87.

18. Cai, X. J., Liu, Z. Q., Chen, M., & An, Q. L. (2012). An experimental investigation on effects of minimum quantity lubrication oil supply rate in high-speed end milling of Ti-6Al-4V. *Proceeding of the Institution of Mechanical Engineers, Part B: Journal Engineering Manufacture, 226*(11), 1784–1792.

19. Liu, Z. Q., Cai, X. J., Chen, M., & An, Q. L. (2011). Investigation of cutting force and temperature of end-milling Ti-6Al-4V with different minimum quantity lubrication (MQL) parameters. *Proceedings of the Institution of Mechanical Engineers, Part B: Journal of Engineering Manufacture, 225*(8), 1273–1279.

20. Wang, C. D., Chen, M., An, Q. L., Wang, M., & Zhu, Y. H. (2014). Tool wear performance in face milling Inconel 182 using minimum quantity lubrication with different nozzle positions. *International Journal of Precision Engineering and Manufacturing, 15*(3), 557–565.

21. Wang, C. Y., Xie, Y. X., Zheng, L. J., Qin, Z., Tang, D. W., & Song, Y. X. (2014). Research on the chip formation mechanism during the high-speed milling of hardened steel. *International Journal of Machine Tools and Manufacture, 79*, 31–48.

22. Jang, D. Y., Jung, J., & Seok, J. (2016). Modeling and parameter optimization for cutting energy reduction in MQL milling process. *International Journal of Precision Engineering and Manufacturing-Green Technology, 3*(1), 5–12.

23. Iyappan, S. K., & Ghosh, A. (2020). Small quantity lubrication assisted end milling of aluminium using sunflower oil. *International Journal of Precision Engineering and Manufacturing-Green Technology, 7*(2), 337–345.

24. Ganguli, S., & Kapoor, S. G. (2016). Improving the performance of milling of titanium alloys using the atomization-based cutting fluid application system. *Journal of Manufacturing Processes, 23*, 29–36.

25. Zhang, Y., & Jun, M. B. G. (2013). Mixed jet of independently atomized water and oil sprays as cutting fluids in micro-milling. *Manufacturing Letters, 1*(1), 13–16.

26. Sun, S., Brandt, M., Palanisamy, S., & Dargusch, M. S. (2015). Effect of cryogenic compressed air on the evolution of cutting force and tool wear during machining of Ti-6Al-4V alloy. *Journal of Materials Processing Technology, 221*, 243–254.

27. Wang, C. Y., Lin, H. S., Wang, X., Zheng, L. J., & Xiong, W. Q. (2017). Effect of different oil-on-water cooling conditions on tool wear in turning of compacted graphite cast iron. *Journal of Cleaner Production, 148*, 477–489.

28. Sales, W. F., Schoop, J., & Jawahir, I. S. (2017). Tribological behavior of PCD tools during superfinishing turning of the Ti6Al4V alloy using cryogenic, hybrid and flood as lubri-coolant environments. *Tribology International, 114*, 109–120.

29. Junior, A. B., Diniz, A. E., & Filho, F. T. (2009). Tool wear and tool life in end milling of 15–5 PH stainless steel under different cooling and lubrication conditions. *The International Journal of Advanced Manufacturing Technology, 43*(7–8), 756–764.

30. Hutchings, I., & Shipway, P. (2017). *Tribology: friction and wear of engineering materials* (2nd ed.). Oxford: Btterworth-Heinemann.

31. Zhang, H., Zhao, J., Wang, F., Zhao, J., & Li, A. (2014). Cutting forces and tool failure in high-speed milling of titanium alloy TC21 with coated carbide tools. *Proceedings of the Institution of Mechanical Engineers, Part B: Journal of Engineering Maufacture, 229*(1), 20–27.

32. Jawaid, A., Sharif, S., & Koksal, S. (2000). Evaluation of wear mechanisms of coated carbide tools when face milling titanium alloy. *Journal of Materials Processing Technology, 99*(1–3), 266–274.

33. Cantero, J. L., Díaz-álvarez, J., Miguélez, M. H., & Marín, N. C. (2013). Analysis of tool wear patterns in finishing turning of Inconel 718. *Wear, 297*(1–2), 885–894.

34. Liew, W. Y. H., & Ding, X. (2008). Wear progression of carbide tool in low-speed end milling of stainless steel. *Wear, 265*(1–2), 155–166.

35. Su, Y., He, N., Li, L., & Li, X. L. (2006). An experimental investigation of effects of cooling/lubrication conditions on tool wear in high-speed end milling of Ti-6Al-4V. *Wear, 261*(7–8), 760–766.

36. Yang, B., Shen, X., & Lei, S. (2009). Mechanisms of edge chipping in laser-assisted milling of silicon nitride ceramics. *International Journal of Machine Tools and Manufacture, 49*(3–4), 344–350.

37. Itoigawa, F., Childs, T. H. C., Nakamura, T., & Belluco, W. (2006). Effects and mechanisms in minimal quantity lubrication machining of an aluminum alloy. *Wear, 260*(3), 339–344.

38. Tai, B. L., Stephenson, D. A., Furness, R. J., & Shih, A. J. (2014). Minimum quantity lubrication (MQL) in automotive powertrain machining. *Procedia CIRP, 14*, 523–528.

39. Werda, S., Duchosal, A., Le Quilliec, G., Morandeau, A., & Leroy, R. (2017). Minimum quantity lubrication advantages when applied to insert flank face in milling. *International Journal of Advanced Manufacturing Technology, 92*(5–8), 2391–2399.

40. Rao, P. N. (2013). *Manufacturing technology: metal cutting and machine tools* (3rd ed.). New Delhi: Tata McGraw-Hill Education.

41. Merchant, M. E. (1945). Mechanics of the metal cutting process. I. Orthogonal cutting and a type 2 chip. *Journal of Applied Physics, 16*(5), 267.

42. Lee, E. H., & Shaffer, B. W. (1951). The theory of plasticity applied to a problem of machining. *Journal of Manufacturing Science and Engineering, Transactions of the ASME, 18*(4), 405–413.

43. Cook, N. H., Jhaveri, P., & Nayak, N. (1963). The mechanism of chip curl and its importance in metal cutting. *Journal of Engineering for Industry, 85*(4), 374–380.

Shixiong Wu is an associate professor in Mechanical and Electrical Engineering Institute, Guangdong University of Technology. He received Ph.D. from Zhejiang University. His research interests mainly include the high-efficiency machining of hardened mold steel, high-speed cutting/high-efficiency grinding theory and application, green manufacturing of the difficult-to-cut materials.

Hongchang Liao is currently pursuing a M.Sc. in mechanical engineering at Guangdong University of Technology. His current research interests include high-efficiency machining theory and green cutting technology of difficult-to-cut materials.

Suyang Li is a lecturer in Mechanical and Electrical Engineering Institute at Guangdong University of Technology. She received her doctorate from Nagoya University in Japan. His research interests mainly include CAE simulation and optimization, plastic forming, neural network, high-speed machining theory and cutting mechanism.

Jundong Bi is a master degree candidate in Guangdong University of Technology. He studies cutting and process technology through experiments and numerical methods. In addition, he focuses on green cutting technology such as liquid nitrogen, oils on water (OoW) and minimum quantity lubrication (MQL).

Zhiyang Li is a master degree candidate in Guangdong University of Technology. His main research directions include green and high-efficiency cutting technology such as oils on water (OoW), minimum quantity lubrication (MQL).